WARSAW UNIVERSITY OF TECHNOLOGY Index 351733
FACULTY OF CIVIL ENGINEERING
COMMITTEE FOR CIVIL AND WATER ENGINEERING
POLISH ACADEMY OF SCIENCES ISSN 1230-2945

DOI: 10.24425/ace.2026.1392

ARCHIVES OF CIVIL ENGINEERING

Vol. LXXII ISSUE 3 2026

 pp. 317 –333

Case study

A case study of terrestrial laser scanning as a data source for 3D modeling for water flow analysis in a small hydropower plant

Piotr Kędziorski[1], Jacek Katzer[2], Paweł Tysiąc[3], Marcin Jagoda[4]

Abstract: The article proposes a methodology for measuring and processing results, integrating data obtained from Terrestrial Laser Scanning (TLS) with Computational Fluid Dynamics (CFD) analyses, aimed at evaluating water flow conditions in a real-world Small Hydropower Plant (SHP) system. Based on TLS data, a detailed 3D model of the SHP (located in Koszalin, Poland) geometry was developed, which was used to conduct a series of numerical simulations in ANSYS Fluent. The analyses covered six water flow variants, including simulated scenarios accounting for different widths of potential dam leakages. The results confirmed that using TLS data as the basis for the geometric model enables the investigation of actual water flow in the hydropower system. The developed 3D SHP model achieved an accuracy of ±0.02 m relative to the acquired point cloud, and the analyses performed based on it allowed for the evaluation of water flow in the system. The study showed that, in the case of a sealed intake chamber, outlet number 2 handles the largest water mass, accounting for 39.2% of the total flow, while outlets number 1 and 3 account for 33.9% and 26.9%, respectively. The proposed use of TLS data for 3D modeling for water flow analyses in SHP systems highlights the significant potential of integrating TLS and CFD as a widely applicable engineering tool.

Keywords: computational fluid dynamics, hydropower, terrestrial laser scanning, TLS

[1]MSc., Eng., Koszalin University of Technology, Faculty of Civil Engineering, Environmental and Geodetic Sciences, Sniadeckich 2, 75-453 Koszalin, Poland, e-mail: piotr.kedziorski@tu.koszalin.pl, ORCID: 0000-0001-7753-2388
[2]DSc., PhD., Eng., University of Warmia and Mazury in Olsztyn, Faculty of Geoengineering, Prawochenskiego 15, 10-720 Olsztyn, Poland, e-mail: jacek.katzer@uwm.edu.pl, ORCID: 0000-0002-4049-5330
[3]PhD., Eng., Gdansk University of Technology, Faculty of Civil and Environmental Engineering, Gabriela Narutowicza 11/12, 80-233 Gdansk, Poland, e-mail: pawel.tysiac@pg.edu.pl, ORCID: 0000-0002-5017-4522
[4]DSc., PhD., Eng., Koszalin University of Technology, Faculty of Civil Engineering, Environmental and Geodetic Sciences, Sniadeckich 2, 75-453 Koszalin, Poland, e-mail: marcin.jagoda@tu.koszalin.pl, ORCID: 0000-0001-8073-6242

1. Introduction

Small Hydropower Plants (SHPs) are a key component of sustainable energy systems, particularly in the context of local utilization of renewable energy sources [1, 2]. Due to their lower environmental impact and the ability to be located within existing hydrotechnical structures, historic facilities such as water mills, weirs, or dams are increasingly being adapted to serve as SHPs [3]. The efficiency and safety of their operation depend on the precise mapping of water flow conditions and the analysis of the system's structural components [4–6]. Modern measurement technologies, such as Terrestrial Laser Scanning (TLS), can provide comprehensive information about the geometry of such structures. In recent years, there has been a dynamic increase in the use of TLS for documenting hydrotechnical facilities [7–9]. This technology enables rapid and precise acquisition of three-dimensional spatial data regarding the geometry of dams, pipelines, technical equipment, and surrounding terrain [10, 11]. With its high resolution and point cloud density, TLS facilitates the creation of detailed 3D models, which are applied not only in object inventory but also in various technical and engineering analyses. Previous studies have primarily focused on the assessing the geometry of structures, analyzing deformations, subsidence, and other parameters directly related to the technical condition of hydrotechnical facilities [7, 9, 12–18]. For example, Dreier et al. [19] demonstrated the potential of using unmanned aerial vehicles (UAVs) equipped with LiDAR scanners as an alternative to terrestrial measurements. Meanwhile, Kang et al. [20] presented an integrated approach combining UAV and TLS data to assess the technical condition of a dam. In the work of Xu et al. [21], a NURBS surface model was developed based on TLS data, showing that this technology can be used to study the stability and deformation of hydrotechnical structures using precise geometric models.

Three-dimensional spatial models are a valuable source of information for technical analyses of hydrotechnical structures. One of the tools supporting such analyses is Computational Fluid Dynamics (CFD), which is used to model water flows in complex structural systems. CFD methods are widely applied in studies of dams, channels, pipelines, and water turbines, enabling the simulation of velocity distributions, pressure, streamlines, and other hydrodynamic parameters without the need for costly physical experiments [22, 23]. In engineering practice, these analyses are often based on simplified design models or technical documentation, which can limit the accuracy of representing actual geometric and flow conditions [23–29]. This creates a research gap, particularly regarding the use of data obtained from terrestrial laser scanning as a direct source of geometric information for numerical water flow analyses in hydrotechnical structures [30, 31]. Previous studies have primarily focused on using TLS for inventory purposes, deformation monitoring, or assessing the technical condition of hydrological structures, but they have not addressed the integration of this data with CFD to model water flows in the actual geometry of hydrotechnical facilities.

The aim of this study is to develop a three-dimensional geometric model of a SHP, including its hydraulic system, based on TLS data, and to conduct CFD numerical analyses to determine the distribution of velocity and water flow under operational conditions, as well as in scenarios involving dam leakages. The proposed approach, combining real geometry with numerical simulation, enables a more accurate assessment of hydrodynamic conditions, identification of potential energy losses, and structural irregularities in the hydrotechnical facility. The presented solution can be applied in technical diagnostics, planning modernization, and designing hydrotechnical structures, while also demonstrating the potential for integrating geodetic measurement techniques with computational engineering tools.

2. SHP chosen for scanning

The subject of the study is an SHP located in Koszalin, Poland, at the site of a former water mill. The location of the facility is shown in Fig. 1.

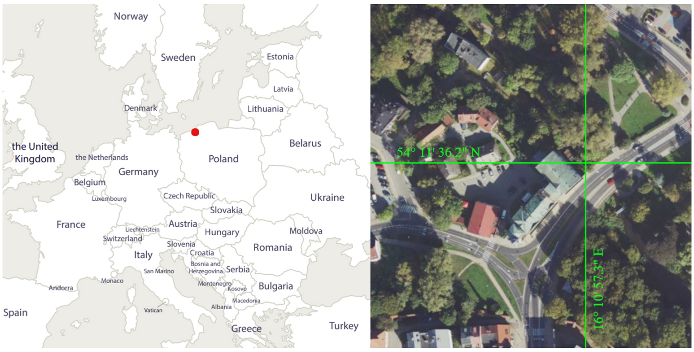

Fig. 1. Location of the SHP

The history of the facility dates back to 1266, when the first mill structures were established. The current form of the complex was shaped between 1838 and 1842, when a water mill was constructed on the site of the earlier structure based on a design by Krahn. In 1878, the mill was equipped with a water turbine. At the beginning of the 20th century, plans were made to adapt it for electricity production, which was realized in 1924. After World War II, between 1945 and 1946, the mill's equipment was dismantled, and in the following years, the building served as a warehouse. Currently, the former mill houses the District Museum, while the dam has been adapted for the purposes of the Small Hydropower Plant. The SHP is equipped with three pump-turbines, each with a capacity of 45 kW, operating at an average flow rate of approximately 1 m^3/s and a water head of 6 meters [32–34].

3. Measurement method

The SHP was surveyed using the Z+F Imager 5016 terrestrial laser scanner from Zoller & Fröhlich (Wangen im Allgäu, Germany). The device is a phase- based scanner capable of recording point clouds at ranges from 0.3 m to 365 m. The operational range depends on surface reflectivity and atmospheric conditions. The maximum data acquisition speed is 1.1 million points per second. The distance measurement accuracy is ≤ 1 mm±10 ppm/m. The angular resolution can reach 0.00018°, resulting in high data density when scanning from short distances. The horizontal field of view is 360°, and the vertical field of view is 320°. The scanner is equipped with an integrated IMU system, which enables stabilization and spatial orientation of the data, improving registration quality when working with multiple scan stations. The survey using the terrestrial scanner consisted of nine scan stations. Eight of the scan stations were located outside the SHP and one was located inside the machine room, where the plant's technical equipment is housed. Details, of the locations of all nine scan stations are presented in Fig. 2.

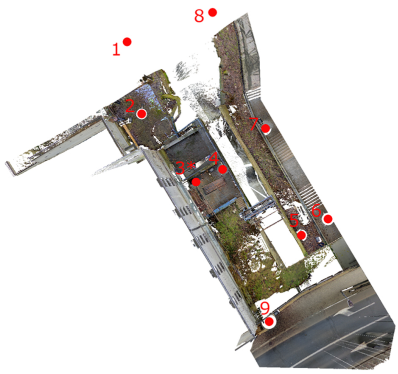

Fig. 2. Locations of scan stations (* – inside the machine room)

The acquired measurement data were initially processed in Z+F Laser Control Scout software (version 9.1.0) and then exported in .e57 format. Each scan contained approximately 170 million points. The prepared data were imported into CloudCompare software (version 2.13.1) to remove measurement noise and limit the data scope to the area under analysis. The point clouds were then merged and resampled, maintaining a minimum distance between points of 0.005 m. The purpose of resampling was to generalize the data and eliminate overlapping points from different scan stations. The final point cloud consisted of 43,388,189 points and was exported in .e57 format. Fig. 3 illustrates the appearance of the resulting point cloud. This methodology was successfully harnessed by the research team in previous research programs regarding to the degradation of cultural heritage objects [35, 36].

Fig. 3. The appearance of the resulting point cloud

4. 3D modeling

The processed point cloud was imported into Rhinoceros 8 (version 8 SR17) software, where 3D modeling of the object was performed. The modeling process involved manual reconstruction of the small hydropower plant's geometry and associated technical infrastructure based on spatial data. The modeling was based on mapping the main planes and curvatures of the object, utilizing surface and solid operations available in the Rhino environment. To ensure geometric consistency, surface fitting to points and tools for reconstructing edges from cross-sectional and longitudinal sections were used. Infrastructure elements not visible in the point cloud, such as certain parts of technical equipment, intakes, or internal components, were modeled based on technical documentation and information provided by the plant operator. During the modeling stage, simplifications were applied to architectural details that did not significantly impact subsequent analyses. In addition to the model representing the plant's geometry (Fig. 4), a model of the water flow space within the SHP system, corresponding to the volume filled with water, was also developed. The geometric model served as the basis for further numerical analyses conducted in the CFD environment. It was developed in three variants, differentiated by the configuration of the flow system.

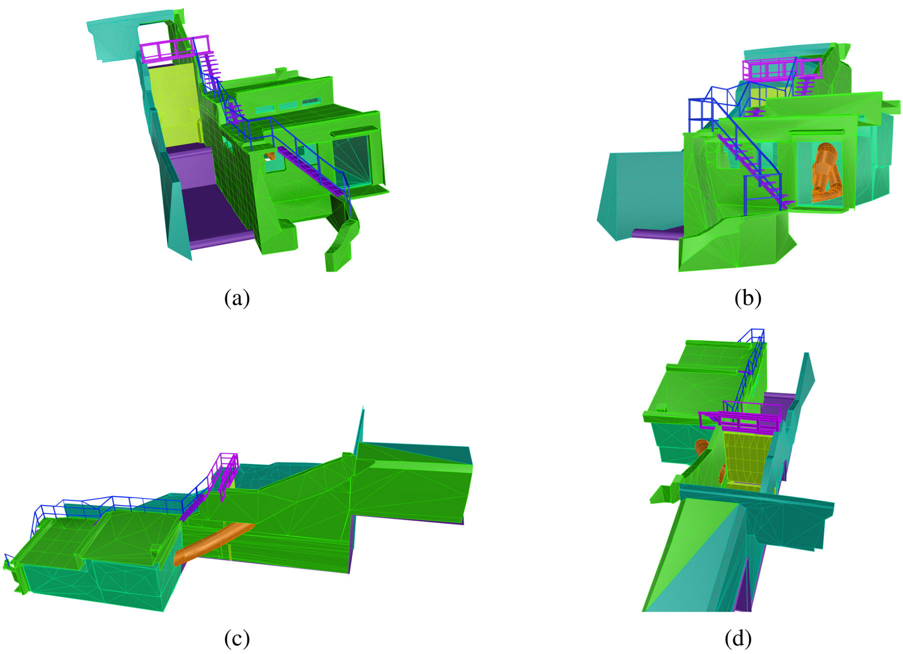

Fig. 4. Achieved 3D Mode: (a) View from the northwest side, (b) View from the west side, (c) View from the southwest side, (d) View from the southeast side

5. CFD analysis

Numerical simulations of water flow in the SHP system were conducted using ANSYS software (version 2025 R1) with the Fluent model (version 2025 R1.04), based on a previously prepared 3D geometric model imported in .STP format. The computational mesh was generated directly in the Fluent environment using the built-in tool. Six variants of water flow simulations in the SHP system were performed. The first variant, analyzed water flow solely in the pipeline supplying water to the turbines (see Fig. 5). The second variant, included both the pipeline and the intake chamber, assuming a fully closed dam (see Fig. 6). The third variant, analyzed the intake chamber and pipeline, model, considering a simulated dam leakage, resulting in water flow through its lower part (see Fig. 7). This variant was evaluated for three cases, varying the overflow height at 8 cm, 6 cm, and 4 cm (overflows smaller than 4 cm were not detectable).

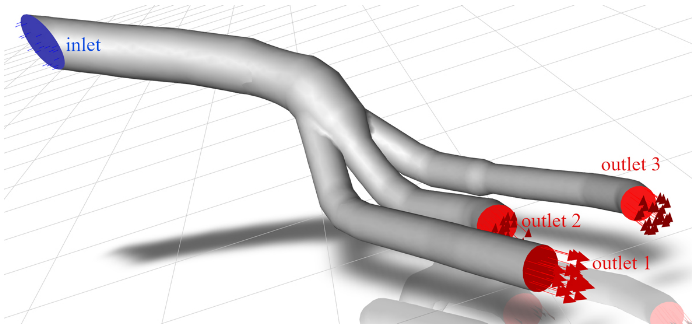

Fig. 5. Model of the flow space for Variant I – the pipeline supplying water from the intake chamber to the inlets
of the pump-turbines

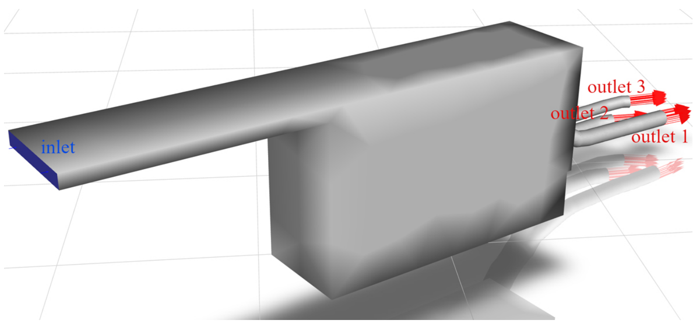

Fig. 6. Model of the flow space for Variant II – the intake chamber and supply pipeline, assuming a fully closed dam with no flow through its upper part

The analysis was conducted in steady-state mode, accounting for gravity. A mass-flow inlet boundary condition of 200 kg/s was applied at the inlet, aligned with the pipeline axis. The outlets were defined with a pressure- outlet condition at a reference pressure of 0 Pa.

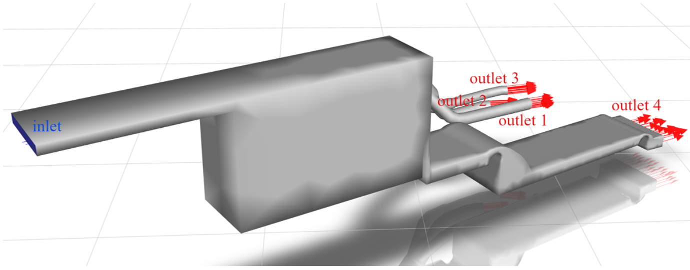

Fig. 7. Model of the flow space for Variant III – the intake chamber and supply pipeline, assuming a dam overflow

All model walls were defined as impermeable with a no-slip condition. The $k - \varepsilon$ (standard) model was used for turbulent flow modeling. The material assigned to the flow domain was water-liquid from the ANSYS Fluent database. The computational process was initiated with Compute From Inlet initialization, and calculations were performed for 500 iterations using the SIMPLE solving scheme and second-order accuracy (Second Order). The obtained results include velocity distributions within the chamber and supply pipeline, as well as the volume of water passing through each of the four outlets. The simulations enabled the assessment of the impact of geometry and potential leakages on the nature of water flow under conditions close to real-world scenarios.

An analysis of grid independence was conducted to evaluate the impact of computational grid resolution on simulation results for variant two. Six grid scenarios with maximum element sizes ranging from 2.4 to 0.075 meters were considered. The densest mesh, containing over 780,000 elements, served as the reference. Detailed results are shown in Table 1 and Table 2.

For the grid with a maximum size of 0.6 meters (adopted for all variants in this study), the differences from the reference solution are as follows: Outlet 1: –3.9% velocity and -3.7% mass flow; Outlet 2: –1.6% velocity and –0.9% mass flow; and Outlet 3: +6.6% velocity and +6.5% mass flow.

Table 1. Effect of mesh size on outlet velocity

Max mesh element size [m]	Number of faces	Outlet_1 Velocity [m/s]	Δ Outlet_1 Velocity [%]	Outlet_2 Velocity [m/s]	Δ Outlet_2 Velocity [%]	Outlet_3 Velocity [m/s]	Δ Outlet_3 Velocity [%]
2.4	79552	0.309	–9.1%	0.379	–1.6%	0.439	13.9%
, 1.2	82060	0.311	–8.6%	0.372	–3.3%	0.451	16.9%
0.6*	83931	0.327	–3.9%	0.379	–1.6%	0.411	6.6%
0.3	99544	0.342	0.6%	0.378	–1.9%	0.388	0.6%
0.15	193866	0.345	1.5%	0.376	–2.4%	0.389	1.0%
0.075	780823	0.340	Reference	0.385	Reference	0.385	Reference

Δ – deviation from the reference value (0.075 m); ∗ – value selected for further analysis.

Table 2. Effect of mesh size on outlet mass flow

Max mesh element size [m]	Number of faces	Outlet_1 Mass Flow [kg/s]	Δ Outlet_1 Mass Flow [%]	Outlet_2 Mass Flow [kg/s]	Δ Outlet_2 Mass Flow [%]	Outlet_3 Mass Flow [kg/s]	Δ Outlet_3 Mass Flow [%]
2.4	79552	–64.019	–9.1%	–78.507	–0.7%	–57.469	13.8%
1.2	82060	–64.289	–8.7%	–76.703	–3.0%	–58.993	16.8%
0.6 *	83931	–67.830	–3.7%	–78.384	–0.9%	–53.778	6.5%
0.3	99544	–70.512	0.2%	–78.572	–0.6%	–50.902	0.8%
0.15	193866	–71.036	0.9%	–77.946	–1.4%	–50.944	0.9%
0.075	780823	–70.406	Reference	–79.085	Reference	–50.500	Reference

Δ – deviation from the reference value (0.075 m); * – value selected for further analysis.

6. Analysis of the results

The first stage of the analysis was to evaluate the accuracy of the geometric representation of the SHP in the developed 3D model. To this end, a comparison was made between the 3D model and the original point cloud. Since the point cloud covered a larger area than the model itself, points with a distance from the model's surface exceeding ±0.5 m were filtered out to standardize the comparison. As a result, a point cloud consisting of 14,618,671 points was obtained, as shown in Fig. 8. The points were visualized using a color scale to facilitate the interpretation of deviations, ranging from -0.05 m to 0.05 m. Points with deviations beyond this range were marked in gray. Detailed statistics of the point cloud are presented in Table 3. The analysis showed that approximately 70% of the points fall within a deviation range of ±0.02 m, which can be considered the average accuracy of the SHP geometry representation. Points with larger errors are mainly located on secondary objects, such as technical equipment, window curtains, rods, grates, or tools hanging on walls, which were not included in the model due to their insignificance for the conducted research.

Table 3. Detailed statistics of the point cloud

Deviation range [m]	Number of points	Percent of points [%]
–0.005; 0.005	4711312	32.23%
–0.01; 0.01	8794150	60.16%
–0.02; 0.02	10255887	70.16%
–0.03; 0.03	10822268	74.03%
–0.04; 0.04	11003622	75.27%
–0.05; 0.05	11219783	76.75%
–0.10; 0.10	11878592	81.26%
–0.20; 0.20	12862210	87.98%
–0.30; 0.30	13606904	93.08%
–0.40; 0.40	14237039	97.39%
–0.50; 0.50	14618671	100.00%

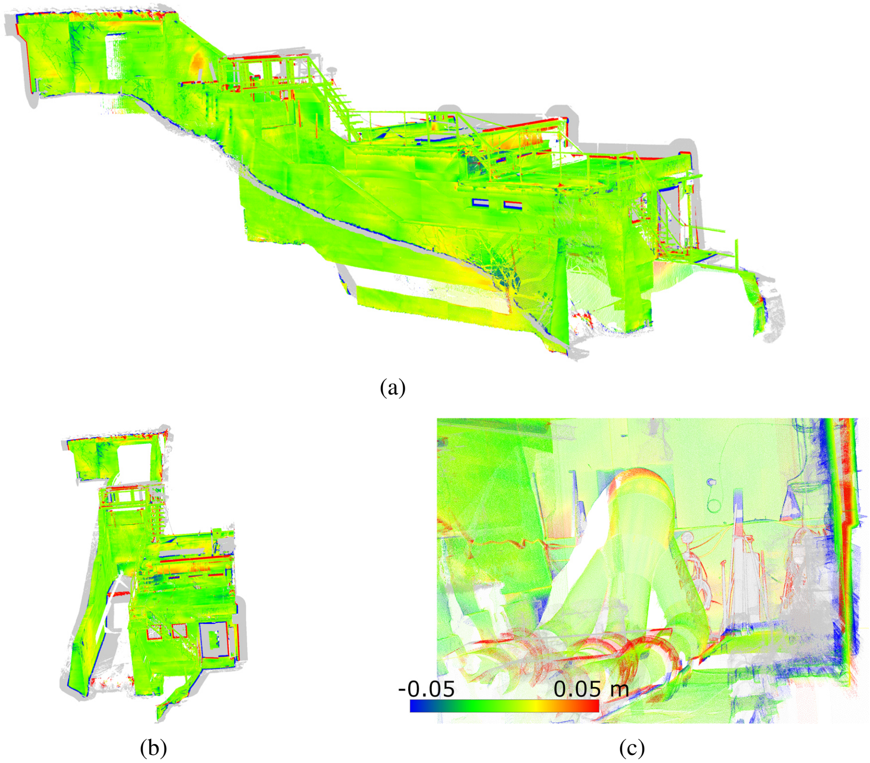

Fig. 8. Point cloud with the interpretation of deviations: (a) View from the north side, (b) View from the northwest side, (c) View of the interior of the object

The second stage of the analysis involved assessment of the water flow in the SHP system to determine the velocity and volume of water passing through each of its outlets. Detailed results are presented in Table 4. The analysis revealed that in Variant I, which includes only the pipeline supplying water to the three turbines, the total mass flow is distributed unevenly among the outlets: the largest share is attributed to Outlet 2 (80.5 kg/s), while the smallest is at Outlet 1 (57.4 kg/s). In Variant II, which additionally includes the intake chamber, a more balanced flow distribution is observed, although Outlet 2 still has the largest share. This is due to its position relative to the main pipeline, as it forms a direct extension of it, causing the water stream to be directed primarily toward Outlet 2. The other outlets, positioned at an angle, receive part of the flow after a change in the stream's direction. Variant III, simulating dam leakages (three cases of overflow), shows a clear reduction in flow through the three main outlets (Outlets 1-3), which is a direct consequence of the additional flow through Outlet 4, capturing overflow water. As the overflow height decreases (from 8 cm to 4 cm), the flow through Outlet 4 diminishes, resulting in an increased share of water directed to the other outlets. For example, with a overflow of 8 cm height, Outlet 4 accounts for over 40% of the total flow (81.0 kg/s), while for a 4 cm overflow height, it accounts for about 32% (63.7 kg/s).

Table 4. Volume of wate er passing thr rough each of o SHP outlet ts

		Inlet	Outlet 1	Outlet 2	Outlet 3	Outlet 4
Variant I	Velocity [m/s]	0.187	0.281	0.413	0.472	–
	Area [m2]	1.073	0.208	0.208	0.131	–
	Mass Flow [kg/s]	200.000	–57.443	–80.544	–62.014	–
Variant II	Velocity [m/s]	0.267	0.327	0.379	0.411	–
	Area [m2]	0.750	0.208	0.208	0.131	–
	Mass Flow [kg/s]	200.000	–67.830	–78.384	–53.778	–
Variant III – 8 cm	Velocity [m/s]	0.267	0.199	0.229	0.231	0.076
	Area [m2]	0.750	0.208	0.208	0.131	1.374
	Mass Flow [kg/s]	200.000	–41.242	–46.793	–30.439	–80.966
Variant III – 6 cm	Velocity [m/s]	0.267	0.215	0.249	0.231	0.068
	Area [m2]	0.750	0.208	0.208	0.131	1.374
	Mass Flow [kg/s]	200.000	–44.524	–51.482	–30.095	–73.648
Variant III – 4 cm	Velocity [m/s]	0.267	0.224	0.260	0.263	0.060
	Area [m2]	0.750	0.208	0.208	0.131	1.374
	Mass Flow [kg/s]	200.000	–46.551	–53.875	–34.736	–63.714

An interesting phenomenon is the change in water flow velocity through Outlet 1 between Variants I and II. Despite the larger inlet surface area in Variant I (1.073 m^2 compared to 0.750 m^2 in Variant II) and a lower inlet velocity (0.187 m/s vs. 0.267 m/s), the water velocity at Outlet 1 is lower in Variant I, while velocities at Outlets 2 and 3 are higher. This phenomenon results from the direction of water inflow. In Variant I, which includes only the pipeline, water enters perpendicular to the inlet surface, causing the stream to collide with the side wall (Wall 1 – Fig. 9) and then move along it. This flow direction favors water being directed to Outlets 2 and 3, while limiting inflow to Outlet 1. In Variant II, which includes the intake chamber, water enters the pipeline after gaining flow direction within the chamber's space. This creates a gentle vortex in the pipeline, promoting a more even distribution of water across the entire cross-section. As a result, the flow through all three outlets becomes more balanced, as illustrated in Fig. 9.

The visualizations of velocity distributions in the cross-sections of Outlets 1-3, shown in Fig. 10, allow observation of the variability in flow structure. In the variant including only the pipeline (Fig. 10), the maximum velocity is distributed relatively unevenly, with increased flow intensity in the middle and upper parts of the cross-sections. The flow distribution is asymmetric due to the inlet water direction discussed above. In the variant with the intake chamber and a fully closed dam (Fig. 11), the flow shows a more uniform velocity profile. Subsequent cases (Fig. 12) with 8, 6, and 4 cm overflows reveal increasing outlet velocities as the overflow narrows.

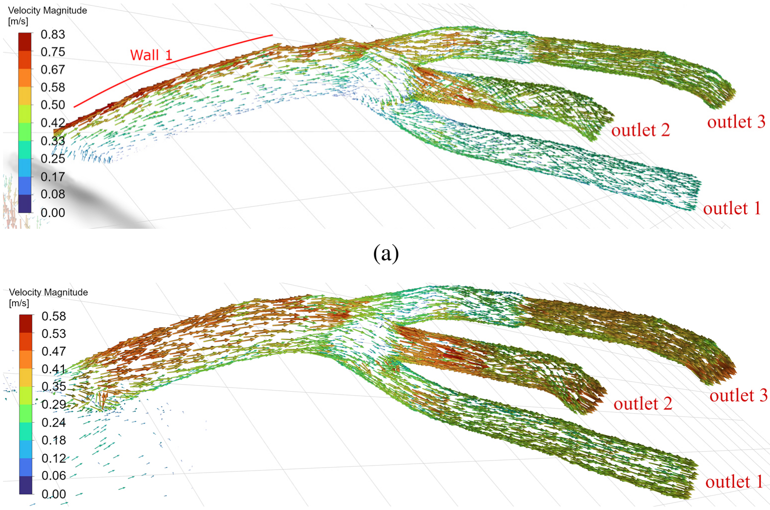

(a)

(b)

Fig. 9. Water flow directions: (a) Simulation for Variant I, (b) Simulation for Variant II

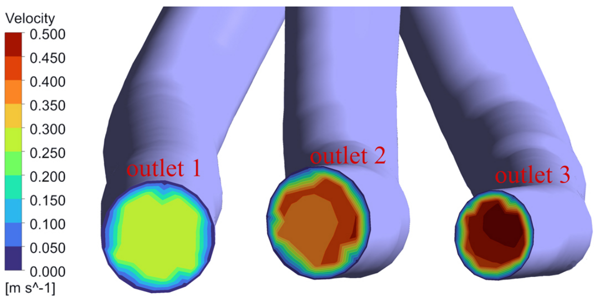

Fig. 10. Velocity distribution at Outlets 1-3 for Variant I

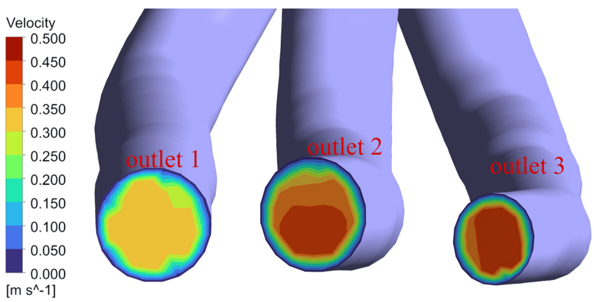

Fig. 11. Velocity distribution at Outlets 1-3 for Variant II

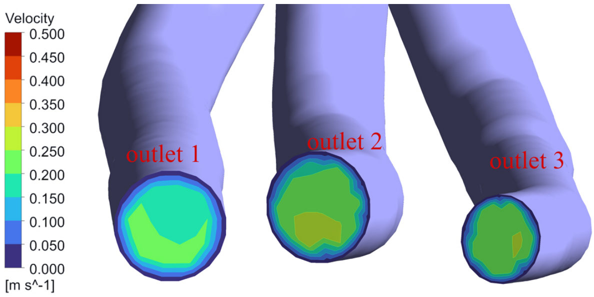

Fig. 12. Velocity distribution at Outlets 1-3 for Variant III at overflow of 8 cm

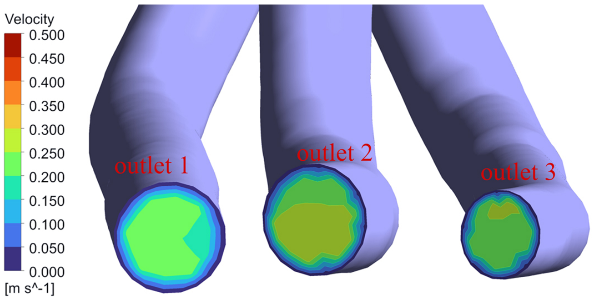

Fig. 13. Velocity distribution at Outlets 1-3 for Variant III at overflow of 6 cm

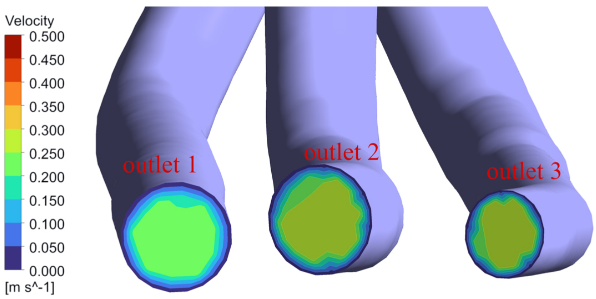

Fig. 14. Velocity distribution at Outlets 1-3 for Variant III at overflow of 4 cm

To better illustrate the distribution of mass flow among the outlets, Table 5 presents the results as percentages relative to the total water flow at the inlet.

In Variant I, Outlet 2 plays a dominant role, handling over 40% of the total water stream. The introduction of the intake chamber (Variant II) results in a partial shift of water flow from Outlet 3 to Outlet 1. Variant III (simulating dam overflow) shows a systematic reduction in water flow through the additional outlet, Outlet 4, as the overflow height decreases (8 cm to 4 cm). Meanwhile, the flow distribution among Outlets 1-3 remains similar to that observed in Variant II.

Table 5. Percentage share of outf flow relative to the total water flow at t the inlet

	Mass Flow	Inlet	Outlet 1	Outlet 2	Outlet 3	Outlet 4
Variant I	[kg/s]	200.000	–57.443	–80.544	–62.014	–
	[%]	100.00%	–28.72%	–40.27%	–31.01%	–
Variant II	[kg/s]	200.000	–67.830	–78.384	–53.778	–
	[%]	100.00%	–33.92%	–39.19%	–26.89%	–
Variant III 8 cm	[kg/s]	200.000	–41.242	–46.793	–30.439	–80.966
	[%]	100.00%	–20.62%	–23.40%	–15.22%	–40.48%
Variant III 6 cm	[kg/s]	200.000	–44.524	–51.482	–30.095	–73.648
	[%]	100.00%	–22.26%	–25.74%	–15.05%	–36.82%
Variant III 4 cm	[kg/s]	200.000	–46.551	–53.875	–34.736	–63.714
	[%]	100.00%	–23.28%	–26.94%	–17.37%	–31.86%

7. Discussion

The presented research confirm the effectiveness of using data obtained through TLS to construct 3D geometric models of hydrotechnical structures, which subsequently serve as a robust foundation for computational fluid dynamics analyses. The accuracy of the developed 3D model, determined through comparison with the point cloud, indicates that approximately 70% of the points fall within a deviation range of ±0.02 m. This result demonstrates that, with an appropriately conducted generalization and simplification process, it is possible to obtain a model that faithfully represents the actual shape of the object. Converting the full point cloud into a generalized yet accurate spatial model significantly facilitates further data processing, reducing data volume and computational complexity without substantial loss of geometric quality.

The use of a 3D model based on the actual geometry of the object enabled detailed numerical analyses, covering six water flow variants in the SHP system. This allowed for the determination of velocity and mass flow values at each outlet, providing insights into the behavior of water flow under different geometric configurations. The first analyzed variant, considering only the pipeline, highlighted significant limitations of simplified models. Due to the perpendicular inflow direction relative to the inlet plane, the flow was distinctly asymmetric, with the dominant portion of the stream directed toward Outlets 2 and 3, while the flow through Outlet 1 was significantly limited. Such a phenomenon, difficult to predict without detailed knowledge of the inlet direction and the actual geometry of the entire system, underscores the limitations of analyses based solely on models representing fragments of the complete hydraulic system. Similar conclusions were drawn by Souček et al. [31], who emphasized that the optimal approach for flow modeling involves using a digital twin derived from scanning data, encompassing the full geometry of the analyzed object.

Incorporating the intake chamber (Variant II) allowed for a more natural shaping of the water stream before entering the pipeline, resulting in a more balanced flow among the three outlets. This demonstrates that realistic representation of the full geometry is crucial for accurately capturing flow phenomena in hydrotechnical structures. Even minor changes in the configuration of inflow elements can affect the final distribution of flow streams, thus impacting the overall efficiency of the system. Our proposed approach for studying water flow in SHPs, based on TLS data and CFD analyses, enables the reconstruction of the object's geometry and a better understanding of flow mechanisms in existing, often irregular, hydraulic systems. The need for developing such an approach was highlighted by Machalski et al. [30], who presented the construction of a digital twin of a hydropower plant, emphasizing the importance of acquiring 3D spatial data to more accurately model the current geometry of the object, which may differ from that indicated in available technical documentation.

In the analyses of Variant III, it was demonstrated that the proposed approach can be successfully used to simulate potential structural leakages and assess their impact on flow parameters in the hydraulic system. Incorporating dam leakages of varying simulated widths allowed for the observation of changes in water flow distribution, particularly a significant reduction in mass flows directed to the turbines. A portion of the water was diverted to a new outflow channel (Outlet 4), which in real- world conditions could lead to reduced efficiency of the energy system. A similar approach was employed in the studies by Akinyemi and Liu [25], where simulations enabled the evaluation of the impact of different geometric configurations on energy efficiency. Our simulations showed that the method integrating TLS data and CFD modeling enables the assessment of the effects of local geometric defects, making it a valuable tool for technical diagnostics and planning maintenance work in existing hydrotechnical structures.

A certain limitation of the conducted analyses is the assumption of specific water flow conditions and the omission of some geometric details. The developed model accurately represents the structure of the object and preserves key features of the hydraulic system, but a generalized form was deliberately adopted to reduce computational complexity. In future work, it is possible to further increase the accuracy of geometric representation, for instance, by incorporating wall roughness, minor structural elements, and local surface irregularities, which may influence flow characteristics under real operational conditions. Despite the adopted simplifications, the obtained results confirm that TLS data can serve as a reliable source of geometric information for CFD analyses of real hydrotechnical systems.

The conducted simulations have additional limitations, including the use of a steady-state approach, which assumes time-invariant flow conditions. Although this method is commonly used in preliminary engineering analyses because of its lower computational cost and shorter processing time, it cannot represent dynamic phenomena occurring in the system, such as pressure pulsations, transient changes in velocity distribution, or localized vortex formation [37]. In real turbine operations, these effects may impact system efficiency and structural wear. Using a steady-state model in this study was a deliberate simplification motivated by the primary objective of demonstrating the feasibility of using TLS-derived 3D geometry as input data for CFD analysis. As such, certain modeling simplifications were adopted intentionally.

8. Conclusions

Based on the conducted research program, the following conclusions can be drawn:

- The obtained results indicate that the use of TLS data enables precise reconstruction of the flow system's geometry and can serve as a foundation for hydrodynamic analyses. The simulations demonstrated a significant influence of the actual shape of inflow elements on the nature of water flow, particularly evident when comparing the simplified variant (pipeline only) with the model incorporating the intake chamber.

- The accuracy of the developed 3D model compared to the point cloud was ±0.02 m for approximately 70% of the points, confirming the suitability of the proposed approach for creating faithful geometric models that can be used for further engineering analyses.
- The analysis of the variant with simulated dam overflow demonstrated the ability to assess the impact of structural defects on the water balance of the system and its energy efficiency. When simulating an 8 cm dam overflow, Outlet 4 captured over 40% of the total water stream, highlighting the importance of such analyses in evaluating the performance of existing SHPs.
- The conducted analyses underscore the potential of the proposed approach, which integrates TLS data and CFD simulations. The developed methodology can be successfully applied in research and engineering tasks, particularly in cases where complete technical documentation is lacking or when local geometric irregularities need to be considered. It can be valuable for diagnosing the technical condition and modernizing small hydropower facilities.

References

[1] N. Walczak, „Operational Evaluation of a Small Hydropower Plant in the Context of Sustainable Development", *Water*, vol. 10, no. 9, art. no. 1114, 2018, doi: 10.3390/w10091114.

[2] B. Dursun and C. Gokcol, „The role of hydroelectric power and contribution of small hydropower plants for sustainable development in Turkey", *Renewable Energy*, vol. 36, no. 4, pp. 1227–1235, 2011, doi: 10.1016/j.renene.2010.10.001.

[3] T.B.A. Couto and J.D. Olden, „Global proliferation of small hydropower plants – science and policy", *Frontiers in Ecology and the Environment*, vol. 16, no. 2, pp. 91–100, 2018, doi: 10.1002/fee.1746.

[4] H.S. Sachdev, A.K. Akella, and N. Kumar, „Analysis and evaluation of small hydropower plants: A bibliographical survey", *Renewable and Sustainable Energy Reviews*, vol. 51, pp. 1013–1022, 2015, doi: 10.1016/j.rser.2015.06.065.

[5] S. Mishra, S.K. Singal, and D.K. Khatod, „Optimal installation of small hydropower plant—A review", *Renewable and Sustainable Energy Reviews*, vol. 15, no. 8, pp. 3862–3869, 2011, doi: 10.1016/j.rser.2011.07.008.

[6] D. Borkowski and T. Węgiel, „Small Hydropower Plant With Integrated Turbine- Generators Working at Variable Speed", *IEEE Transactions on Energy Conversion*, vol. 28, no. 2, pp. 452–459, 2013, doi: 10.1109/TEC.2013.2247605.

[7] L. Ramos-Alcázar, M. Marchamalo-Sacristán, and R. Martínez-Marín, „Estimating and Plotting TLS Midrange Precisions in Field Conditions: Application to Dam Monitoring", *International Journal of Civil Engineering*, vol. 15, no. 2, pp. 299–307, 2017, doi: 10.1007/s40999-016-0093-3.

[8] X.-Y. Ning, et al., „3D deformation analysis for earth dam monitoring based on terrestrial laser scanning (TLS) and the iterative closest point (ICP) algorithm", *Frontiers in Earth Science*, vol. 12, art. no. 1421705, 2024, doi: 10.3389/feart.2024.1421705.

[9] S. Zhao, F. Kang, J. Li, and C. Ma, „Structural health monitoring and inspection of dams based on UAV photogrammetry with image 3D reconstruction", *Automation in Construction*, vol. 130, art. no. 103832, 2021, doi: 10.1016/j.autcon.2021.103832.

[10] J. Teng, Y. Shi, H. Wang, and J. Wu, „Review on the Research and Applications of TLS in Ground Surface and Constructions Deformation Monitoring", *Sensors*, vol. 22, no. 23, art. no. 9179, 2022, doi: 10.3390/s22239179.

[11] E. Kaartinen, K. Dunphy, and A. Sadhu, „LiDAR-Based Structural Health Monitoring: Applications in Civil Infrastructure Systems", *Sensors*, vol. 22, no. 12, art. no. 4610, 2022, doi: 10.3390/s22124610.

[12] G. Buffi, P. Manciola, S. Grassi, M. Barberini, and A. Gambi, "Survey of the Ridracoli Dam: UAV-based photogrammetry and traditional topographic techniques in the inspection of vertical structures", *Geomatics, Natural Hazards and Risk*, vol. 8, no. 2, pp. 1562–1579, 2017, doi: 10.1080/19475705.2017.1362039.

[13] B. Kwoczyńska and B. Małysa, "Integration of data obtained from laser scanning and UAV used to develop a 3D model of the building object", *Archives of Civil Engineering*, vol. 68, no. 4, pp. 311–330, 2022, doi: 10.24425/ace.2022.143040.

[14] P. Martínez-Carricondo, F. Carvajal-Ramírez, L. Yero-Paneque, and F. Agüera- Vega, "Combination of HBIM and UAV photogrammetry for modelling and documentation of forgotten heritage. Case study: Isabel II dam in Níjar (Almería, Spain)", *Heritage Science*, vol. 9, art. no. 95, 2021, doi: 10.1186/s40494-021-00571-8.

[15] E. Ridolfi, G. Buffi, S. Venturi, and P. Manciola, "Accuracy Analysis of a Dam Model from Drone Surveys", *Sensors*, vol. 17, no. 8, art. no. 1777, 2017, doi: 10.3390/s17081777.

[16] G. Lenda, N. Borowiec, and U. Marmol, "Study of the Precise Determination of Pipeline Geometries Using UAV Scanning Compared to Terrestrial Scanning, Aerial Scanning and UAV Photogrammetry", *Sensors*, vol. 23, no. 19, art. no. 8257, 2023, doi: 10.3390/s23198257.

[17] M.E. Kowalska, J. Zaczek-Peplinska, and Ł. Piasta, "Determining the trend of geometrical changes of a hydrotechnical object based on data in the form of LiDAR point clouds", *Archives of Civil Engineering*, vol. 70, no. 1, pp. 305–323, 2024, doi: 10.24425/ace.2024.148913.

[18] C. Suchocki, M. Damięcka-Suchocka, and M. Jagoda, "Determination of the building wall deviations from the vertical plane", in *Proceedings of the 7th International Conference Environmental Engineering, 22-23 May 2008, Vilnius, Lithuania*. Vilnius Gediminas Technical University Press, 2008, pp. 1488–1492.

[19] A. Dreier, H. Kuhlmann, and L. Klingbeil, "The potential of UAV-based Laser Scanning for Deformation Monitoring – Case Study on a Water Dam", in *Proceedings of the 5th Joint International Symposium on Deformation Monitoring (JISDM), 20-22 June 2022, Valencia, Spain*. Technical University of Valencia (UPV), 2022, pp. 261–269, doi: 10.4995/JISDM2022.2022.13833.

[20] J. Kang, D. Kim, C. Lee, J. Kang, and D. Kim, "Efficiency Study of Combined UAS Photogrammetry and Terrestrial LiDAR in 3D Modeling for Maintenance and Management of Fill Dams", *Remote Sensing*, vol. 15, no. 8, art. no. 2026, 2023, doi: 10.3390/rs15082026.

[21] H. Xu, L. Haibo, X. Yang, S. Qi, and J. Zhou, "Integration of Terrestrial Laser Scanning and NURBS Modeling for the Deformation Monitoring of an Earth-Rock Dam", *Sensors*, vol. 19, no. 1, art. no. 22, 2018, doi: 10.3390/s19010022.

[22] G. Ardizzon, G. Cavazzini, and G. Pavesi, "A new generation of small hydro and pumped-hydro power plants: Advances and future challenges", *Renewable and Sustainable Energy Reviews*, vol. 31, pp. 746–761, 2014, doi: 10.1016/j.rser.2013.12.043.

[23] Z. Krzemianowski and M. Kaniecki, "Low-head high specific speed Kaplan turbine for small hydropower – design, CFD loss analysis and basic, cavitation and runaway investigations: A case study", *Energy Conversion and Management*, vol. 276, art. no. 116558, 2023, doi: 10.1016/j.enconman.2022.116558.

[24] D. Liszka, et al., "Alternative Solutions for Small Hydropower Plants", *Energies*, vol. 15, no. 4, art. no. 1275, 2022, doi: 10.3390/en15041275.

[25] O.S. Akinyemi and Y. Liu, "CFD modeling and simulation of a hydropower system in generating clean electricity from water flow", *International Journal of Energy and Environmental Engineering*, vol. 6, no. 4, pp. 357–366, 2015, doi: 10.1007/s40095-015-0180-2.

[26] M.V. Nikolić, R.M. Karamarković, M.V. Karamarković, and V.M. Karamarković, "Retrofit of a settling basin of a small hydropower plant", *Engineering Structures*, vol. 236, art. no. 112118, 2021, doi: 10.1016/j.engstruct.2021.112118.

[27] O.S. Abdullah, A.H. Kamel, and W.H. Khalil, "Numerical and Experimental Modelling of Small Hydropower Turbine", *Journal of Advanced Research in Fluid Mechanics and Thermal Sciences*, vol. 80, no. 1, pp. 112–127, 2021, doi: 10.37934/arfmts.80.1.112127.

[28] B. Alapfy, N.F. Gamarra, and N. Rüther, "Towards Hydraulic Design Optimization of Shaft Hydropower Plants: A 3D-CFD Application Based on Physical Models", *Water*, vol. 16, no. 19, art. no. 2790, 2024, doi: 10.3390/w16192790.

[29] M. Nikolić, V. Karamarković, R. Karamarkovic, and M. Marašević, "Design improvement of a side water intake on a small hydropower plant", in *Proceedings of the Ninth International Triennial Conference HEAVY MACHINERY (HM 2017), 28 June – 1 July 2017, Zlatibor, Serbia*. Kraljevo: Faculty of Mechanical and Civil Engineering, 2017, pp. 51–57.

[30] A. Machalski, et al., "The Concept of a Digital Twin for the Wały Śląskie Hydroelectric Power Plant: A Case Study in Poland", *Energies*, vol. 18, no. 8, art. no. 2021, 2025, doi: 10.3390/en18082021.

[31] J. Souček, P. Nowak, M. Kantor, and R. Veselý, "CFD as a Decision Tool for Pumped Storage Hydropower Plant Flow Measurement Method", *Water*, vol. 15, no. 4, art. no. 779, 2023, doi: 10.3390/w15040779.

[32] W. Witek, "Watermills and windmills in the cultural landscape of Western Pomerania", *Zeszyty Siemczyńsko-Henrykowskie*, vol. 4, pp. 55–70, 2014 (in Polish).

[33] W. Witek and M. Witek, "Watermills in Western Pomerania (sources of historical energy)", in *Z nurtem rzeki. Au fil de l'eau*. Szczecin: Biuro Dokumentacji Zabytków, 2014, pp. 29–47 (in Polish).

[34] "Hazard analysis, including identification of places where there is a risk to the safety of people using water areas for swimming, bathing, practicing sports or recreation in the City of Koszalin", Municipality Office of Koszalin. [Online]. Available: https://www.koszalin.pl/sites/default/files/pliki/analiza_zagrozen_na_akwenach_-_07.06.2024.pdf. [Accessed: 04 Apr. 2025] (in Polish).

[35] P. Kędziorski, M. Jagoda, P. Tysiąc, and J. Katzer, "An Example of Using Low-Cost LiDAR Technology for 3D Modeling and Assessment of Degradation of Heritage Structures and Buildings", *Materials*, vol. 17, no. 22, art. no. 5445, 2024, doi: 10.3390/ma17225445.

[36] M. Damięcka-Suchocka, J. Katzer, and C. Suchocki, "Application of TLS Technology for Documentation of Brickwork Heritage Buildings and Structures", *Coatings*, vol. 12, no. 12, art. no. 1963, 2022, doi: 10.3390/coatings12121963.

[37] Y. Chande, "Investigation on CFD Analysis Practices for Predicting Flow in Centrifugal Fan Using Steady State and Transient Analysis", in *Proceedings of the 7th International and 45th National Conference on Fluid Mechanics and Fluid Power (FMFP), 10-12 December 2018, Mumbai, India*. 2018.

Studium przypadku wykorzystania naziemnego skaningu laserowego jako źródła danych do modelowania 3D w celu analizy przepływu wody w małej elektrowni wodnej

Słowa kluczowe: energia wodna, naziemny skaning laserowy, obliczeniowa mechanika płynów, TLS

Streszczenie:

W artykule zaproponowano metodologię pomiaru i opracowania jego wyników integrującą dane pozyskane za pomocą naziemnego skaningu laserowego (TLS) z analizami numerycznymi typu CFD (Computational Fluid Dynamics), mającą na celu ocenę warunków przepływu wody w rzeczywistym układzie Małej Elektrowni Wodnej (MEW). Na podstawie danych TLS opracowano szczegółowy model 3D geometrii obiektu – MEW w Koszalinie, Polska, który posłużył do przeprowadzenia serii symulacji numerycznych w środowisku ANSYS Fluent. Analizy objęły sześć wariantów przepływu wody, w tym symulowane scenariusze uwzględniające różne szerokości potencjalnych nieszczelności zapory. Wyniki badań potwierdziły, że wykorzystanie danych TLS jako podstawy modelu geometrycznego pozwala na zbadanie rzeczywistego przepływu wody w układzie elektrowni. Opracowany model 3D MEW osiągnął dokładność ±0,02 m względem pozyskanej chmury punktów, a wykonane na jego podstawie analizy umożliwiły ocenę przebiegu wody w systemie. Badania wykazały, że w przypadku szczelnej komory ujęciowej odpływ numer 2 przyjmuje największe masy wody, wynoszące 39,19% całkowitego przepływu, natomiast odpływy numer 1 i 3 odpowiednio 33,92% i 26,89%. Zaproponowane w pracy wykorzystanie danych TLS do modelowania 3D na potrzeby analiz przepływu wody w układzie MEW wskazuje na duży potencjał integracji TLS i CFD jako narzędzia inżynierskiego o szerokim zastosowaniu.

Received: 2025-09-24, Revised: 2025-10-30